Nanoscale

PAPER

View Article Online
View Journal | View Issue

Cite this: *Nanoscale*, 2017, **9**, 5323

Metal–polydopamine frameworks and their transformation to hollow metal/N-doped carbon particles†

Y. Liang,[a] J. Wei,‡[a] Y. X. Hu,[a] X. F. Chen,[a] J. Zhang,[b] X. Y. Zhang,[c] S. P. Jiang,[b] S. W. Tao[a] and H. T. Wang*[a]

Received 9th February 2017,
Accepted 22nd March 2017

DOI: 10.1039/c7nr00978j

rsc.li/nanoscale

We present a new strategy for *in situ* transformation of metal–organic framework (MOF) crystals to hollow metal–organic structures through polycondensation of dopamine. The hollow metal–polydopamine (PDA) particles are formed by a coordination assembly of metal ions (Co and Zn) and PDA, inheriting the morphology of MOF (ZIF-67 and ZIF-8) crystals. The hollow porous metal/N-carbon particles morphosynthetically transformed from hollow metal–PDA particles exhibit excellent oxygen reduction electrocatalytic activity. The strategy presented here is promising for synthesizing hollow metal–organic polymer (metal–carbon) particles with diverse morphologies for energy and environmental applications.

Introduction

Nanoporous carbon materials have attracted much attention due to their chemical and mechanical stability, high surface area, good electrical conductivity and various applications such as in catalysis, adsorption, separation, energy conversion and storage, as well as environmental remediation.[1–7] In particular, nanoporous carbon materials with hollow structures can further enhance their performance in many applications.[8–13] In general, hollow carbon nanoparticles are synthesized *via* the templating technique, which usually involves the coating of a carbon precursor on a pre-synthesized solid core template (such as silica colloids, polystyrene spheres), followed by carbonization and selective removal of the templates.[14–16] However, the removal of the template is time-consuming and involves some harmful solvents (such as HF). Furthermore, to satisfy different applications, extra functionalization is needed, such as introducing heteroatoms into hollow carbon particles.[17] The doping of nitrogen atoms into the nanoporous carbon materials changes the properties of carbon, such as surface polarity, electrical conductivity and electron-donor tendency.[18] For example, N doped carbon materials have been shown to have efficient catalytic activity toward oxygen reduction reaction (ORR), which is an important electrode reaction in fuel cells and metal–air batteries.[19–24] Additionally, introducing transition metal ions (such as Co and Fe) into N-doped carbon can remarkably boost the catalytic performance of ORR due to the formation of M–N–C (M=Fe, Co) active sites.[25–27] To produce a hollow M–N–C containing structure, metal ions or N elements are typically introduced into the hollow carbon structure by extra procedures,[28,29] which would easily cause uneven distribution and agglomeration after carbonization. Thus, developing an efficient way to synthesize functional hollow carbon materials containing homogeneous active sites is highly desirable.

Metal–organic frameworks (MOFs), assembled by metal ion clusters and organic ligands,[30–36] show various morphologies and compositions and tuneable particle size, which are suitable templates for the synthesis of a hollow structure.[32,37–41] MOF materials were demonstrated as sacrificial templates to synthesize hollow oxide composites or metal composites.[42] Nevertheless, hollow carbon materials directly derived from metal–organic coordination complexes have been rarely reported.[9,23] MOFs are attractive candidates for the synthesis of metal–carbon composites due to their diverse compositions with various metal ions and organic ligands.[43–46] For example, zeolite imidazolate frameworks (ZIFs), a subclass MOFs, are the most commonly-used precursor for carbon-based catalysts as they are rich in carbon, nitrogen and transition metal elements, which could form M–N–C active sites after carbonization to improve the catalytic performance in electrochemical catalysis. However, MOF precursors with hollow structures are

[a]*Department of Chemical Engineering, Monash University, Clayton, Vitoria 3800, Australia. E-mail: huanting.wang@monash.edu*
[b]*Fuels and Energy Technology Institute & Department of Chemical, Engineering, Curtin University, Perth, WA 6102, Australia*
[c]*School of Chemistry, Monash University, Clayton, Victoria 3800, Australia*
†Electronic supplementary information (ESI) available. See DOI: 10.1039/c7nr00978j
‡Present address: The Key Laboratory of Biomedical Information Engineering of Ministry of Education, School of Life Science and Technology, Xi'an Jiaotong University, Xi'an, Shaanxi 710049, P. R. China.

quite limited,[47] especially unique morphology, such as a polyhedral MOF structure. Therefore, synthesis of diverse hollow metal/carbon structures is still a challenge and desirable for fabrication of high-performance carbon-based catalysts.

Herein, we demonstrate a novel strategy for synthesizing hollow metal–organic structures from MOF crystals, involving *in situ* polycondensation of dopamine into polydopamine (PDA) and a coordination assembly of metal ions with PDA to form the shell, and simultaneous release of organic ligand molecules to produce the hollow structure. Hollow metal–PDA particles inherit the shape of MOFs and their shell is composed of PDA and metal ions originated from MOFs. In other words, the formation of the hollow structure and the introduction of heteroatoms into particles are achieved in one step. In previous research, PDA has been often utilized to functionalize the surface of MOF crystals since it can easily self-polymerize from dopamine.[8,48] However, the PDA assisted *in situ* transformation of an MOF into a hollow metal/PDA complex has never been reported. On the other hand, the MOFs not only function as morphology templates but also supply metal ions to coordinate with the PDA forming metal–PDA shell structure because of their strong chelating capability between PDA and metal ions.[49] Moreover, PDA contains nitrogen and is widely used as an N-doped carbon source. The hollow metal–PDA structures can be further morphosynthetically transformed into porous carbon materials by high temperature carbonization. In this work, two common ZIFs, ZIF-67 and ZIF-8, are chosen to demonstrate the synthesis strategy. After the carbonization, homogeneously dispersed metal–N–C active sites render the carbon materials with high surface area superior catalysts for ORR in alkaline solution.

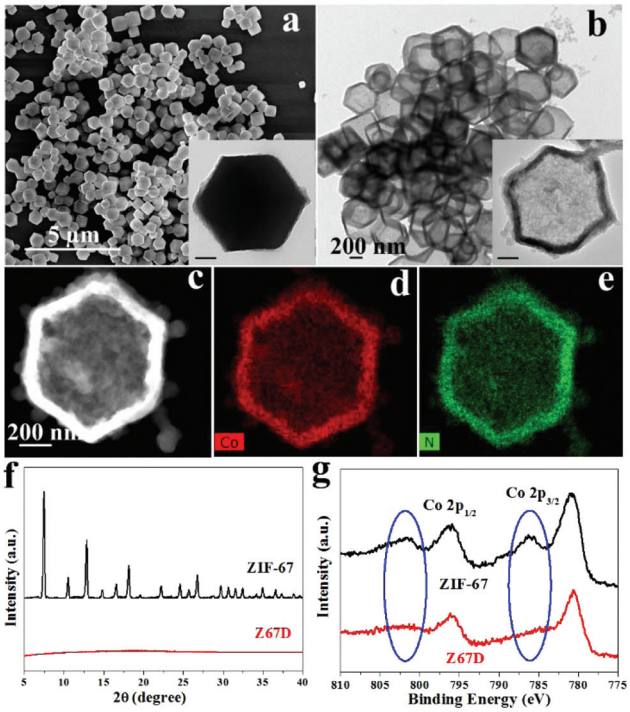

Fig. 1 (a) SEM image of ZIF-67, (b) TEM images, (c) STEM image and (d, e) elemental mapping images of the hollow Co-PDA structure (Z67D) (inset images in (a) and (b) are TEM images of single particles of ZIF-67 and Z67D, respectively. The scale bars represent 100 nm, (f) XRD patterns and (g) XPS spectrum of ZIF-67 and Z67D.

Results and discussion

Rhombic dodecahedron-shaped ZIF-67 crystals with sizes of around 500 nm synthesized from Co^{2+} and 2-methylimidazole (2-mim) are shown in scanning electron microscopy (SEM) and transmission electron microscopy (TEM) images in Fig. 1a. The one-step transformation reaction was initiated by adding dopamine to a suspension of ZIF-67 in a mixture solution (pH 8.5) of ethanol and water, and the reaction occurred at room temperature for 48 h. Fig. 1b shows the TEM images of the product obtained by *in situ* transformation of ZIF-67. The average particle size does not change significantly after transformation. The 50 nm shell of the hollow polyhedral structure (noted as Z67D) was formed by a coordination assembly between Co ions and PDA. As shown in Fig. S1,† the smooth surface of ZIF-67 becomes much rougher in Z67D whose surface is assembled by tiny Co–PDA polymer nanoparticles. To confirm this, Co^{2+} ions were mixed with dopamine in the mixture solution, and spherical nanoparticles of around 20 nm in diameter were produced. The size and shape of these nanoparticles in Fig. S2† are similar to the surface appearance of Z67D, which confirms that the surface of Z67D is formed by coordination between Co^{2+} ions and PDA. Fig. 1c–e show that the existence of the Co element in the shell of the hollow structure was verified by performing scanning transmission electron microscopy (STEM) measurements combined with elemental mapping and energy-dispersive X-ray spectroscopy (EDS) (Fig. S3†). The images show that Co, N and C elements are homogeneously distributed within the shell structure. X-ray powder diffraction (XRD) patterns in Fig. 1f show that the characteristic peaks of the ZIF-67 structure disappear completely in Z67D, indicating that ZIF-67 was fully transformed into Z67D. Moreover, Co 2p X-ray photoelectron spectroscopy (XPS) spectra in Fig. 1g give the peaks of Co $2p_{3/2}$ and Co $2p_{1/2}$ located at around 780 eV and 796 eV for ZIF-67 and Z67D, respectively. Compared with ZIF-67, the two satellite peaks centered at about 786 eV and 802 eV, which are attributed to the Co^{2+} oxidation state, disappear in the spectrum of Z67D. This result indicates that a portion of Co^{2+} ions changes to Co^{3+},[50] which confirms the disappearance of ZIF-67.

To understand the mechanism of transformation from ZIF-67 to Z67D, the reaction process was monitored by characterizing the particles at different reaction stages with TEM (Fig. 2a–d) and XRD (Fig. S4†). ZIF-67 particles were wrapped around by a thin flocculent layer of polydopamine after adding dopamine to the solution for 5 min. A layer of shell was then observed after 30 min. The rate of polymerization of dopamine can be tuned by varying the ratio of water and ethanol.[51] The uniform coverage of PDA on ZIF-67 particles was then

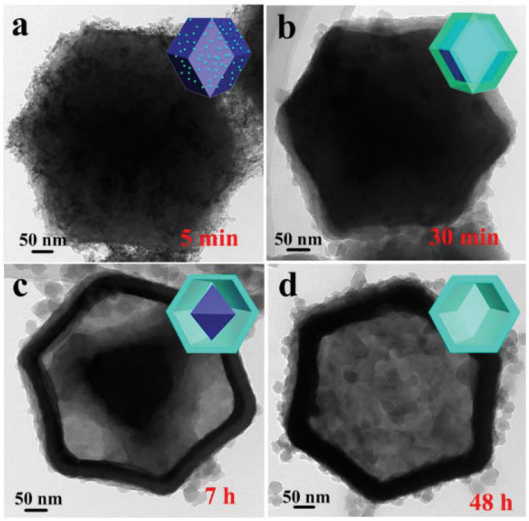

Fig. 2 TEM images of the hollow Z67D structure formed in water and ethanol solution at each stage.

obtained. After 7 h of the reaction, the core of ZIF-67 was dissolved partially, and rhombic dodecahedron-shaped particles with distinct shells were formed. Finally, rhombic dodecahedral hollow particles with a clear shell were observed after 48 h. Furthermore, the Fourier transform infrared (FTIR) spectra of ZIF-67, Z67D and PDA were collected to identify the surface functional groups and observe the formation of a coordination polymer. As shown in Fig. S5a,† the broad band around 3338 cm^{-1} is ascribed to the N–H and O–H stretching vibrations in PDA and Z67D.[52] The band at 1590 cm^{-1} in ZIF-67 could be assigned to the C=N stretching mode which disappears in Z67D.[53] The absorption band at 420 cm^{-1} originating from the Co–N stretching mode in ZIF-67 disappears in Z67D, demonstrating that Co disaggregates with 2-mim.[54] The Brunauer–Emmett–Teller (BET) surface area of ZIF-67 decreased dramatically, further confirming the disappearance of the ZIF-67 structure and the formation of Z67D (Fig. S5b†).

On the basis of the above observation, the mechanism of the hollow structure formation can be schematically illustrated in Fig. 3. Firstly, the ZIF-67 crystals dissociate in water. The pH

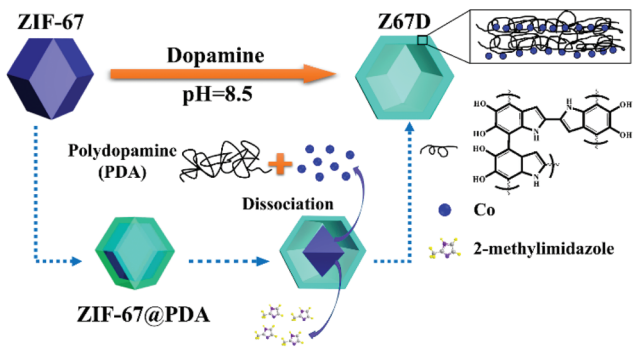

Fig. 3 Schematic illustration of *in situ* transformation from ZIF-67 crystals into hollow Co–PDA polyhedral particles (Z67D).

of the ZIF-67 suspension changes when the ZIF-67 to water mass ratio varies.[55] When the pH decreases, the 2-mim linkers become protonated, which breaks the Co–2-mim bonds.[56] To confirm ZIF-67 hydrolysis in water, ZIF-67 was stirred in a mixed water and ethanol solution (pH = 8.5) and ethanol without adding dopamine for 24 h, respectively. The ZIF-67 structure mostly collapsed into pieces in the mixed solution, but maintained the morphology in ethanol solution (Fig. S6a and b†). This observation indicates that water can destabilize the ZIF-67 structure, releasing Co^{2+} and 2-mim. The second reason is the adsorption ability of dopamine (and PDA) and the competing reaction with Co^{2+} between PDA and 2-mim. As the adsorption of PDA on ZIF-67 is faster than the dissociation of ZIF-67, a thin layer PDA is formed around the ZIF-67 at the beginning to maintain the original polyhedron shape. When Co^{2+} ions released from the breaking of Co–2-mim bonds during water dissolution of ZIF-67, they coordinate with PDA resulting in the formation of a hollow structure with PDA and a Co–PDA layer. To further confirm this conclusion, the hollow Z67D structure was mixed with 6 M HCl and stirred at room temperature for 24 h. The morphology of the structures was still retained with a shell thickness of 25 nm, as shown in Fig. S7a–b.† During the acid treatment, the Co^{2+} ions were removed by the acid and the hollow structures are made of PDA, which is confirmed by the elemental mapping results shown in Fig. S7c–e.† Therefore, Co^{2+} ions released by ZIF-67 coordinate catechol ligands of PDA; meanwhile this coordination reaction further drives Co^{2+} ions to dissociate from 2-mim in solution. These two factors act synergistically, evolving ZIF-67 into a hollow Co–PDA structure in the presence of PDA. Additionally, the concentration of Co^{2+} ions is inversely proportional to the concentration of ZIF-67. When the concentration of a mixture of ZIF-67 and dopamine was increased 10 times that of the Z67D synthesis conditions, the core–shell structures were obtained, as shown in Fig. S8a–e.† The core is incompletely dissociated ZIF-67 which is confirmed by XRD in Fig. S8f.†

Importantly, this transformation strategy can be applied to other ZIFs to prepare hollow metal–polymer structures. For example, a hollow Zn–PDA structure (denoted as Z8D) was synthesized from small-size ZIF-8 nanoparticles (60 nm) (Fig. 4a and b). The elemental mapping images (Fig. 4c) show that Zn and N exist homogeneously in the shell of hollow structures, which is in accordance with the result of Z67D. The average size of hollow particles is around 120 nm, which is due to the formation of a Zn–PDA shell with a thickness of around 40 nm. The characteristic peaks of ZIF-8 disappear in the XRD pattern of Z8D (Fig. 4d), which confirms that the crystalline ZIF-8 transforms into the hollow Zn–PDA structure. The FTIR spectra of ZIF-8 and Z8D proved the disassociation between Zn and 2-mim and coordination of Zn–PDA as shown in Fig. S9.† SEM images in Fig. S10† display the formation process of the hollow Z8D structure.

The CoN_x–C has recently been shown to be an efficient active catalytic site of ORR.[4,20,23] Since the hollow Co/N carbon spheres derived from hollow Co–PDA particles contain both Co

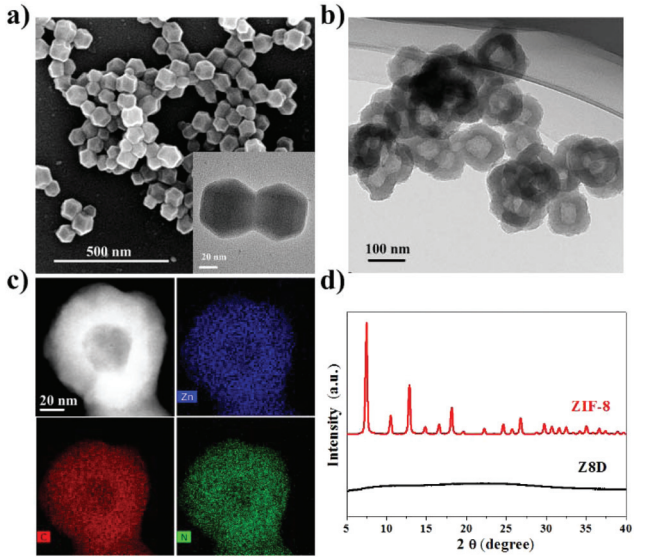

Fig. 4 (a) SEM and TEM (inset image) images of ZIF-8, (b) TEM image, (c) the STEM and elemental mapping images of the hollow Zn–PDA structure (Z8D), and (d) XRD patterns of ZIF-8 and the hollow Z8D structure.

and nitrogen pristinely, it would be interesting to study their chemical structure and ORR catalytic activity. The TEM images in Fig. S11† show that Co/CoN$_x$ is homogeneously dispersed throughout the hollow structure after carbonization of Z67D at 700 °C. After the acid leaching process to remove inactive Co species, the morphology of the hollow structure was still well retained (denoted as Z67D-700-L) (Fig. 5a and S12†). The existence of Co and N in Z67D-700-L was proved by XPS and elemental mapping in Fig. S13.† In the high-resolution spectrum of Co 2p, the peaks of Co–N$_x$ and Co–O species, which can enhance ORR catalytic activity under alkaline conditions,[18,57,58] were identified. The N 1s XPS of Z67D-700-L in Fig. 5b can be fitted into four types of nitrogen, in which the content of pyridinic nitrogen (398.6 eV) and graphitic nitrogen (401.3 eV) is up to 72.63%. The high content of pyridinic N and graphitic N is desirable because they can help impart higher positive charge density on adjacent carbon atoms and increase the limiting current density by facilitating O_2 adsorption and weakening of O=O bonds.[59,60] Furthermore, pyridinic N and pyrrolic N can coordinate with Co to form Co–N$_x$, which is more active than only N-doped carbon materials for ORR.[20,27] For comparison, hollow Co/N carbon particles carbonized at different temperatures and after acid leaching were also investigated. XRD patterns of hollow Co/N carbon particles prepared at different temperatures in Fig. S14† exhibit a peak at 25° corresponding to (002) diffraction of carbon, suggesting that the higher pyrolysis temperature leads to a higher graphitization degree. The peaks located at 44° and 51° are indexed to the (111) and (200) diffractions of fcc Co originated from residual Co nanoparticles embedded in the carbon shell structure.[61] The nitrogen adsorption–desorption isotherms of hollow Co/N carbon particles in Fig. S15† exhibit a very high nitrogen uptake at low relative pressures, which demonstrates the existence of a large amount of nanopores within the shell. The Brunauer–Emmett–Teller (BET) surface area of hollow Co/N carbon particles (Fig. 5c) decreases with increasing pyrolysis temperature, which can be attributed to the decreasing amount of micropores and the structural collapse of Co–PDA hollow particles during the carbonization process. As indicated by the pore size distribution in Fig. S16,† the micropore volume decreases along with the carbonization temperature.

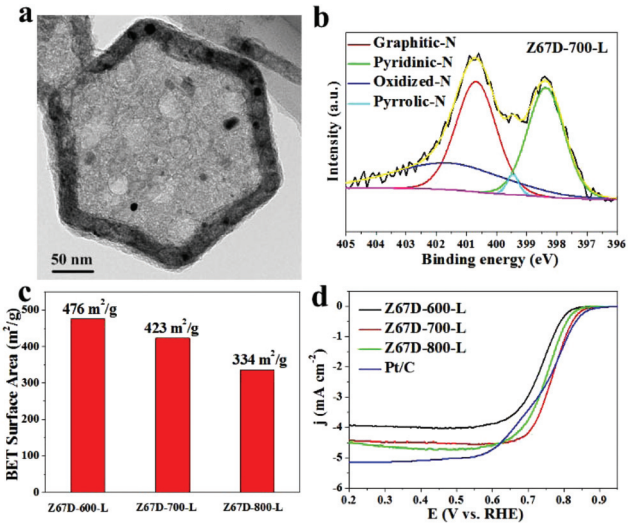

Fig. 5 (a) TEM images of Z67D carbonized at 700 °C after the acid etching process. (b) High-resolution of the N 1s XPS spectra of Z67D-700-L. (c) BET surface area of Z67D-600-L, Z67D-700-L and Z67D-800-L. (d) Linear sweep voltammetry (LSV) curves of Z67D-600-L, Z67D-700-L, Z67D-800-L and Pt/C.

The ORR performance of the hollow Co/N carbon particle electrocatalyst was evaluated by using cyclic voltammetry and rotating disk electrode (RDE) measurements in 0.1 M KOH. Cyclic voltammetry (CV) measurements in an O_2-saturated electrolyte clearly showed oxygen reduction peaks afforded by Z67D-600-L, Z67D-700-L, Z67D-800-L and Pt/C (Fig. S17†). According to the ORR polarization curves in Fig. 5d, the catalytic activity of Z67D-700-L is comparable to Pt/C at the same loading of 0.1 mg cm^{-2} and is the highest among the catalysts carbonized at different temperatures in terms of the half-wave potential. The curves and the corresponding normalized result of different N types in Fig. S18† indicate the conversion from pyrrolic to graphitic nitrogen with increasing temperature, which is consistent with the previous report on N-doped carbon materials.[62] According to the Koutecky–Levich (K–L) plots derived from RDE measurements at different potentials (Fig. S19†), the electron transfer number (n) for Z67D-700-L is 3.5. As shown in Fig. S20,† Z67D-700-L also exhibits great catalytic stability, with a 17.8% activity loss over 10 000 s of continuous operation in O_2 saturated 0.1 M KOH solution, whereas Pt/C suffered around a 40% activity decay under the same conditions. This is because the commercial Pt/C catalyst

suffers from nanoparticle migration, aggregation and even detachment from carbon supports during continuous electrochemical reaction.[63]

Hollow Zn–PDA nanoparticles were also carbonized at 900 °C (denoted as Z8D-900) for testing as ORR electrocatalysts. As shown in Fig. S21,† carbonized Z8D-900 hollow carbon nanoparticles with a size of around 100 nm and uniform nitrogen doping possess a high BET surface area (793 m^2 g^{-1}). Note that elemental Zn evaporated during the high temperature carbonization process.[24] The electrocatalytic performance of Z8D-900, even without metal doping, shown in Fig. S22† is as good as Pt/C, further confirming that hollow PDA is an excellent precursor for the synthesis of electrocatalysts with high catalytic performance.

Conclusions

In summary, we have demonstrated a simple, effective strategy for forming hollow metal–PDA structures from MOF crystals and dopamine. The resulting hollow metal–PDA structure can be readily transformed into hollow metal/N-carbon particles. The method developed in this work avoids an additional step in removing the templates in the synthesis of hollow structures, and achieves well-retained shapes of MOF crystals. Furthermore, the carbonized hollow metal–polymer particles with high surface area and rich active catalytic sites exhibit excellent ORR catalytic performance. Therefore, this versatile method of synthesizing hollow particles has shown great potential for developing novel porous materials for many applications such as in energy and environmental technologies.

Acknowledgements

This work was supported by the Australian Research Council (Discovery Projects DP150100765 and DP150102044). The authors thank the staff of Monash Centre for Electron Microscopy for their technical assistance in SEM and TEM. The authors gratefully acknowledge the assistance of XPS characterization by Jean-Pirerre Veder in the XPS lab at Curtin University and the use of equipment, scientific and technical assistance of the WA X-Ray Surface Analysis Facility, funded by the Australian Research Council LIEF grant LE120100026.

References

1 J. Tang, R. R. Salunkhe, J. Liu, N. L. Torad, M. Imura, S. Furukawa and Y. Yamauchi, *J. Am. Chem. Soc.*, 2015, **137**, 1572–1580.
2 C. Liang, Z. Li and S. Dai, *Angew. Chem., Int. Ed.*, 2008, **47**, 3696–3717.
3 Z. Wu, W. D. Wu, W. Liu, C. Selomulya, X. D. Chen and D. Zhao, *Angew. Chem., Int. Ed.*, 2013, **52**, 13764–13768.
4 Y.-Z. Chen, C. Wang, Z.-Y. Wu, Y. Xiong, Q. Xu, S.-H. Yu and H.-L. Jiang, *Adv. Mater.*, 2015, **27**, 5010–5016.
5 Y. Jiao, Y. Zheng, M. Jaroniec and S. Z. Qiao, *J. Am. Chem. Soc.*, 2014, **136**, 4394–4403.
6 S. J. Yang, M. Antonietti and N. Fechler, *J. Am. Chem. Soc.*, 2015, **137**, 8269–8273.
7 J.-K. Sun and Q. Xu, *Energy Environ. Sci.*, 2014, **7**, 2071–2100.
8 R. Liu, S. M. Mahurin, C. Li, R. R. Unocic, J. C. Idrobo, H. Gao, S. J. Pennycook and S. Dai, *Angew. Chem., Int. Ed.*, 2011, **50**, 6799–6802.
9 S. Yang, L. Peng, P. Huang, X. Wang, Y. Sun, C. Cao and W. Song, *Angew. Chem., Int. Ed.*, 2016, **55**, 4016–4020.
10 C. Liu, J. Wang, J. Li, R. Luo, J. Shen, X. Sun, W. Han and L. Wang, *ACS Appl. Mater. Interfaces*, 2015, **7**, 18609–18617.
11 W. Zhou, X. Xiao, M. Cai and L. Yang, *Nano Lett.*, 2014, **14**, 5250–5256.
12 F. Xu, Z. Tang, S. Huang, L. Chen, Y. Liang, W. Mai, H. Zhong, R. Fu and D. Wu, *Nat. Commun.*, 2015, **6**, 7221.
13 P. Trogadas, V. Ramani, P. Strasser, T. F. Fuller and M.-O. Coppens, *Angew. Chem., Int. Ed.*, 2016, **55**, 122–148.
14 J. Liu, N. P. Wickramaratne, S. Z. Qiao and M. Jaroniec, *Nat. Mater.*, 2015, **14**, 763–774.
15 S. Yang, X. Feng, L. Zhi, Q. Cao, J. Maier and K. Müllen, *Adv. Mater.*, 2010, **22**, 838–842.
16 C. Zhang, H. B. Wu, C. Yuan, Z. Guo and X. W. Lou, *Angew. Chem., Int. Ed.*, 2012, **51**, 9592–9595.
17 J. Wei, Y. Liang, X. Zhang, G. P. Simon, D. Zhao, J. Zhang, S. Jiang and H. Wang, *Nanoscale*, 2015, **7**, 6247–6254.
18 J. Wei, Y. Hu, Y. Liang, B. Kong, J. Zhang, J. Song, Q. Bao, G. P. Simon, S. P. Jiang and H. Wang, *Adv. Funct. Mater.*, 2015, **25**, 5768–5777.
19 M. Lefèvre, E. Proietti, F. Jaouen and J.-P. Dodelet, *Science*, 2009, **324**, 71–74.
20 G. Wu, K. L. More, C. M. Johnston and P. Zelenay, *Science*, 2011, **332**, 443–447.
21 J. Liang, R. F. Zhou, X. M. Chen, Y. H. Tang and S. Z. Qiao, *Adv. Mater.*, 2014, **26**, 6074–6079.
22 W. Niu, L. Li, X. Liu, N. Wang, J. Liu, W. Zhou, Z. Tang and S. Chen, *J. Am. Chem. Soc.*, 2015, **137**, 5555–5562.
23 H. Hu, L. Han, M. Yu, Z. Wang and X. W. Lou, *Energy Environ. Sci.*, 2016, **9**, 107–111.
24 P. Yin, T. Yao, Y. Wu, L. Zheng, Y. Lin, W. Liu, H. Ju, J. Zhu, X. Hong, Z. Deng, G. Zhou, S. Wei and Y. Li, *Angew. Chem., Int. Ed.*, 2016, **55**, 10800–10805.
25 Z. L. Schaefer, M. L. Gross, M. A. Hickner and R. E. Schaak, *Angew. Chem., Int. Ed.*, 2010, **49**, 7045–7048.
26 J. Yuan, C. Giordano and M. Antonietti, *Chem. Mater.*, 2010, **22**, 5003–5012.
27 J. Wei, Y. Liang, Y. Hu, B. Kong, J. Zhang, Q. Gu, Y. Tong, X. Wang, S. P. Jiang and H. Wang, *Angew. Chem., Int. Ed.*, 2016, **55**, 12470–12474.
28 H. Wang, X. Bo, A. Wang and L. Guo, *Electrochem. Commun.*, 2013, **36**, 75–79.
29 L. Chen, L. Zhang, Z. Chen, H. Liu, R. Luque and Y. Li, *Chem. Sci.*, 2016, **7**, 6015–6020.

30 H. Li, M. Eddaoudi, M. O'Keeffe and O. M. Yaghi, *Nature*, 1999, **402**, 276–279.
31 J. S. Seo, D. Whang, H. Lee, S. I. Jun, J. Oh, Y. J. Jeon and K. Kim, *Nature*, 2000, **404**, 982–986.
32 N. Hosono, M. Gochomori, R. Matsuda, H. Sato and S. Kitagawa, *J. Am. Chem. Soc.*, 2016, **138**, 6525–6531.
33 Q.-L. Zhu and Q. Xu, *Chem. Soc. Rev.*, 2014, **43**, 5468–5512.
34 L. E. Kreno, K. Leong, O. K. Farha, M. Allendorf, R. P. Van Duyne and J. T. Hupp, *Chem. Rev.*, 2012, **112**, 1105–1125.
35 P. Horcajada, T. Chalati, C. Serre, B. Gillet, C. Sebrie, T. Baati, J. F. Eubank, D. Heurtaux, P. Clayette, C. Kreuz, J.-S. Chang, Y. K. Hwang, V. Marsaud, P.-N. Bories, L. Cynober, S. Gil, G. Ferey, P. Couvreur and R. Gref, *Nat. Mater.*, 2010, **9**, 172–178.
36 V. P. Santos, T. A. Wezendonk, J. J. D. Jaén, A. I. Dugulan, M. A. Nasalevich, H.-U. Islam, A. Chojecki, S. Sartipi, X. Sun, A. A. Hakeem, A. C. J. Koeken, M. Ruitenbeek, T. Davidian, G. R. Meima, G. Sankar, F. Kapteijn, M. Makkee and J. Gascon, *Nat. Commun.*, 2015, **6**, 6451.
37 N. Yanai, M. Sindoro, J. Yan and S. Granick, *J. Am. Chem. Soc.*, 2013, **135**, 34–37.
38 O. M. Yaghi, M. O'Keeffe, N. W. Ockwig, H. K. Chae, M. Eddaoudi and J. Kim, *Nature*, 2003, **423**, 705–714.
39 S. M. Cohen, *Chem. Rev.*, 2012, **112**, 970–1000.
40 H. Ejima, N. Yanai, J. P. Best, M. Sindoro, S. Granick and F. Caruso, *Adv. Mater.*, 2013, **25**, 5767–5771.
41 B. Y. Xia, Y. Yan, N. Li, H. B. Wu, X. W. Lou and X. Wang, *Nat. Energy*, 2016, **1**, 15006.
42 Z. Jiang, H. Sun, Z. Qin, X. Jiao and D. Chen, *Chem. Commun.*, 2012, **48**, 3620–3622.
43 B. Liu, H. Shioyama, T. Akita and Q. Xu, *J. Am. Chem. Soc.*, 2008, **130**, 5390–5391.
44 A. Comotti, S. Bracco, P. Sozzani, S. Horike, R. Matsuda, J. Chen, M. Takata, Y. Kubota and S. Kitagawa, *J. Am. Chem. Soc.*, 2008, **130**, 13664–13672.
45 S. J. Yang and C. R. Park, *Adv. Mater.*, 2012, **24**, 4010–4013.
46 P. Zhang, F. Sun, Z. Xiang, Z. Shen, J. Yun and D. Cao, *Energy Environ. Sci.*, 2014, **7**, 442–450.
47 X. Xu, F. Nosheen and X. Wang, *Chem. Mater.*, 2016, **28**, 6313–6320.
48 H. Lee, S. M. Dellatore, W. M. Miller and P. B. Messersmith, *Science*, 2007, **318**, 426–430.
49 Y. Liu, K. Ai and L. Lu, *Chem. Rev.*, 2014, **114**, 5057–5115.
50 L. Xu, Q. Jiang, Z. Xiao, X. Li, J. Huo, S. Wang and L. Dai, *Angew. Chem., Int. Ed.*, 2016, **55**, 5277–5281.
51 Q. Yue, M. Wang, Z. Sun, C. Wang, C. Wang, Y. Deng and D. Zhao, *J. Mater. Chem. B*, 2013, **1**, 6085–6093.
52 K. Ai, Y. Liu, C. Ruan, L. Lu and G. Lu, *Adv. Mater.*, 2013, **25**, 998–1003.
53 J. Liu, J. He, L. Y. Wang, R. Li, P. Chen, X. Rao, L. H. Deng, L. Rong and J. D. Lei, *Sci. Rep.*, 2016, **6**, 23667.
54 A. Bigotto, G. Dealti and V. Galasso, *Spectrochim. Acta, Part A*, 1972, **28**, 1581–1591.
55 H. F. Zhang, D. F. Liu, Y. Yao, B. Q. Zhang and Y. S. Lin, *J. Membr. Sci.*, 2015, **485**, 103–111.
56 C. Avci, J. Arinez-Soriano, A. Carne-Sanchez, V. Guillerm, C. Carbonell, I. Imaz and D. Maspoch, *Angew. Chem., Int. Ed.*, 2015, **54**, 14417–14421.
57 A. Aijaz, J. Masa, C. Rösler, W. Xia, P. Weide, A. J. R. Botz, R. A. Fischer, W. Schuhmann and M. Muhler, *Angew. Chem., Int. Ed.*, 2016, **55**, 4087–4091.
58 S. Dou, L. Tao, J. Huo, S. Wang and L. Dai, *Energy Environ. Sci.*, 2016, **9**, 1320–1326.
59 H. W. Liang, X. Zhuang, S. Brüller, X. Feng and K. Müllen, *Nat. Commun.*, 2014, **5**, 4973.
60 K. Gong, F. Du, Z. Xia, M. Durstock and L. Dai, *Science*, 2009, **323**, 760–764.
61 J. Wei, Y. Hu, Z. Wu, Y. Liang, S. Leong, B. Kong, X. Zhang, D. Zhao, G. P. Simon and H. Wang, *J. Mater. Chem. A*, 2015, **3**, 16867–16873.
62 F. Su, C. K. Poh, J. S. Chen, G. Xu, D. Wang, Q. Li, J. Lin and X. W. Lou, *Energy Environ. Sci.*, 2011, **4**, 717–724.
63 Y. Liang, Y. Zhou, J. Ma, J. Zhao, Y. Chen, Y. Tang and T. Lu, *Appl. Catal., B*, 2011, **103**, 388–396.